crystals

MDPI

Article

Oxygen Inhomogeneity and Reversibility in Single Crystal $LaNiO_{3-\delta}$

Hong Zheng [1,*], Bi-Xia Wang [1], D. Phelan [1], Junjie Zhang [2], Yang Ren [3], M. J. Krogstad [1], S. Rosenkranz [1], R. Osborn [1] and J. F. Mitchell [1]

1 Materials Science Division, Argonne National Laboratory, Lemont, IL 60439, USA; Bixia.Wang@anl.gov (B.-X.W.); DPhelan@anl.gov (D.P.); krogstad@anl.gov (M.J.K.); srosenkranz@anl.gov (S.R.); Osborn@anl.gov (R.O.); mitchell@anl.gov (J.F.M.)
2 Institute of Crystal Materials, Shandong University, Jinan, Shandong 250100, China; Junjie@sdu.edu.cn
3 Advanced Photon Source, Argonne National Laboratory, Lemont, IL 60439, USA; Yang@anl.gov
* Correspondence: zheng@anl.gov

Received: 19 May 2020; Accepted: 14 June 2020; Published: 30 June 2020

Abstract: $LaNiO_{3-\delta}$ single crystals have been obtained via high pressure floating zone growth under 149 bar of oxygen pressure. We find a radial gradient in the magnetic properties of specimens extracted from the as-grown boule, which we correlate with the appearance of ordered oxygen vacancy structures. This radial oxygen inhomogeneity has been characterized systematically using a combination of magnetization and X-ray scattering measurements. We establish the presence of rhombohedral ($R\bar{3}c$), oxygen stoichiometric specimens at the periphery of the boule and the presence of a dilute concentration of ordered oxygen-deficient orthorhombic $La_2Ni_2O_5$ in the center. Furthermore, we demonstrate that the as-grown, oxygen-deficient central regions of the crystal can be annealed under high oxygen pressure, without loss of crystallinity, into fully oxygenated $LaNiO_3$, recovering magnetic properties that are characteristic of stoichiometric specimens from the exterior region of the crystal. Thus, single crystals of $LaNiO_{3-\delta}$ possess oxygen content that can be reversibly modified under oxidizing and reducing conditions.

Keywords: nickelates; crystal growth; oxygen deficiency; diffraction

1. Introduction

The subject of the insulator-metal transition in rare-earth perovskite nickelates and its relationship to charge order, antiferromagnetic order, crystal structure, and chemical pressure has been a focal point of research in strongly correlated oxides for decades [1–14]. Nevertheless, it remains an open topic because the mechanism of the transition is still under debate. It has been well-established that the insulating, antiferromagnetic ground state observed for the majority of the rare-earth nickelates becomes progressively less stable as the rare-earth ionic radius increases and as the chemical pressure decreases [15]. Indeed, only $LaNiO_3$, with the largest trivalent rare earth ion [16], does not undergo an insulator-metal transition, but instead remains metallic over the entire measured temperature range [17–19]. Thus, $LaNiO_3$ stands out as having particular importance in nickelate research.

Until very recently, experimental research in bulk materials has been limited to polycrystalline $LaNiO_3$, and the conventional picture has been that in its ground state $LaNiO_3$ is a Pauli-paramagnetic metal [17] subject to Stoner enhancement [2]. However, advances in floating zone growth under oxygen pressure have now made it possible to grow single crystals of $LaNiO_{3-\delta}$ [20–22] and $PrNiO_{3-\delta}$ [23]. In particular, $LaNiO_{3-\delta}$ single crystal growth has been reported by three different research groups: one at Argonne National Laboratory (Lemont, IL, USA) [20], one at the Max Planck Institute (Dresden, Germany) [21], and a third at Heidelberg University (Heidelberg, Germany) [22]. Notably, all three

groups have employed the same high-pressure technique using floating zone furnaces supplied by the same manufacturer, SciDre GmbH, Dresden. However, there are a few surprising experimental features (described below) in the magnetic and thermodynamic properties that have been observed from these crystals that have led to different interpretations of the behavior. In particular, there has been a disagreement regarding whether the observed features are intrinsic to stoichiometric $LaNiO_3$ [21] or an artifact of the incorporation of oxygen-deficient phases that populate the La-Ni-O phase diagram [22,24].

The Argonne group first reported an extremely broad maximum in the magnetic susceptibility (χ) centered at ≈200 K, which had not been reported previously in any polycrystalline or thin film specimen of $LaNiO_3$. This behavior is inconsistent with a conventional Pauli paramagnet [20]. The authors were circumspect about this finding, expressing uncertainty about whether the broad feature was intrinsic to $LaNiO_3$ or an effect of a small, but finite measured oxygen non-stoichiometry [20]. The Dresden group subsequently reported samples that possessed a sharp, bulk antiferromagnetic (AFM) transition at $T_N \approx 150$ K that purportedly appeared in only the most highly stoichiometric specimens [21]. Evidence of this AFM metallic state was provided through anomalies in the magnetic susceptibility (χ) and heat capacity (C_p) as well as through the appearance of an AFM Bragg peak at the expected $\boldsymbol{q} = (\frac{1}{4}\frac{1}{4}\frac{1}{4})$ propagation vector below T_N [21]. Subsequently, the Argonne group showed that such magnetic anomalies could be reproduced in samples by intentionally reducing their oxygen content [24] and attributed these induced anomalies to previously known oxygen-deficient phases [25,26], AFM $LaNiO_{2.5}$ and ferromagnetic (FM) $LaNiO_{2.75}$, the structures of which are displayed in Section I of the Supplementary Materials (SM). More recently, the Heidelberg group likewise concluded that long-range AFM order is not intrinsic to stoichiometric $LaNiO_3$ by examining various pieces of crystals along the axis of crystal growth, observing a correlation between oxygen non-stoichiometry and AFM signatures in the bulk properties [22].

To further characterize this crystal growth and associated oxygen inhomogeneity, we have performed additional experiments to investigate the magnetic and thermodynamic properties of our crystals, focusing on the radial variation of magnetic and structural behavior and its origin in oxygen non-stoichiometry. In particular, we report three findings. First, we find that specimens extracted closest to the axial center exhibit AFM behavior while those taken further out from the center do not. Second, we show that those specimens that do exhibit AFM behavior lose that character when post-growth annealed under high oxygen pressure. Third, the AFM behavior can be reversibly cycled by consecutive annealing treatments under reducing/oxidizing atmospheres. These findings lead to the conclusions that: (1) oxygen stoichiometry is inhomogeneous in both axial and radial growth directions; and (2) this inhomogeneity has a profound influence on the magnetic behavior observed in as-grown specimens and its interpretation.

2. Experimental Details

2.1. Crystal Growth

As-purchased La_2O_3 (Alfa Aesar, 99.99%) was baked at 1,000 °C for 12 h under flowing oxygen before use. Stoichiometric amounts of La_2O_3 and NiO (Alfa Aesar, 99.99%) powder were weighed in a molar ratio of 0.5:1, and the mixture was thoroughly ground, loaded into an Al_2O_3 boat, heated in flowing O_2 to 1050 °C at a rate of 3 °C/min, allowed to dwell for 24 h, and then furnace-cooled to room temperature. The solid was then reground and fired twice at 1050 °C under oxygen, with intermediate grinding, using the same atmosphere and heating protocol. The phases at this point were predominantly a mixture of La_2NiO_4 and NiO without any $LaNiO_{3-\delta}$. The powder was then hydrostatically pressed into polycrystalline rods (length ~80 mm, diameter ~6 mm) at 30,000 psi and sintered at 1050 °C for 24 h under ambient oxygen pressure in preparation for crystal growth. $LaNiO_{3-\delta}$ crystals were grown using the high-pressure floating zone furnace (SciDre GmbH, Dreseden) at Argonne National laboratory. A 5 kW Xenon arc lamp was utilized as a heating source, and growth was carried out under pure oxygen, with pO_2 = 149 bar and a flow rate of 0.2 L/min. We employed a crystal from a previous

50 bar growth as a seed. Feed and seed rods were counter-rotated at 20 and 15 rpm, respectively. The ceramic rod was first densified by traveling through the molten zone at 40 mm/h. From multiple experiments, we have found that feed rod density is critical to success. The densified rod and seed rod were translated at a rate of 4 mm/h for crystal growth, during which the molten zone was stable over more than ten hours. No visible cracks formed during the crystal growth, and only minor volatilization from the growth agents was observed as a faint brown tinge on the quartz tube used as a protective liner for the sapphire pressure containment vessel.

2.2. Single Crystal X-Ray Diffraction

The as-grown crystal boule was characterized using high-energy synchrotron X-ray diffraction at Beamline 11-ID-C of the Advanced Photon Source (APS) at Argonne National Laboratory, with $\lambda = 0.11165$ Å and a beam size of 0.5 mm × 0.5 mm as the sample was rocked over a 10° range. This process was carried out in 5 mm steps from the top to bottom of the boule. Additional measurements were taken on APS Beamline 6-ID-D, with $\lambda = 0.14238$ Å and a 2M CdTe Pilatus detector. Here, the diffraction was recorded with the sample in continuous rotation over an entire 360° range. Three- dimensional reciprocal space was reconstructed using NexPy [27]. The beamline where each dataset was taken is denoted in the figure captions.

2.3. Magnetic Susceptibility

Measurements of χ were carried out using a Quantum Design Magnetic Properties Measurement System (MPMS-3) SQUID magnetometer (Quantum Design, San Diego, CA, USA). An approximately 1 mm thick disc of $LaNiO_{3-\delta}$ crystal was sliced from the crystal boule (≈5 mm from the end of crystal growth) and then cut into several pieces, as shown in Figure 2a. Sequentially, each of these pieces was attached to a quartz rod using a minimum amount of Apiezon grease. Zero-field cooled (ZFC) and field cooled (FC) data were collected under a magnetic field of 0.2 T. The sample was cooled in zero field to 2 K at a rate of 35 K/min, after which the field was applied, and χ was then measured on warming at 2 K/min (ZFC). The sample was subsequently cooled in field at 35 K/min to 2 K, and then χ was measured on warming at 2 K/min (FC).

2.4. Heat Capacity

Measurements of C_p were performed on a Quantum Design Physical Properties Measurement System (PPMS) in the temperature range from 2 to 260 K. Apiezon-N vacuum grease was employed to affix ≈20 mg crystals to the sapphire sample platform. Addenda were subtracted.

2.5. High Pressure Oxygen Annealing

Post-growth, high pressure annealing of the crystals was performed using a high-pressure annealing furnace (Model AHSO) manufactured by SciDre GmbH, Dresden. In this process, the sample was heated under 150 bar of oxygen at 120 °C/h to approximately 600 °C, held at 600 °C for 12 h, and then slowly cooled to 200 °C at 5 °C /h and then 100 °C/h to room temperature, at which point the pressure was reduced to zero over 90 min.

3. Results and Discussion

Figure 1a shows the as-grown single crystal boule of $LaNiO_{3-\delta}$ that we obtained from growth at $pO_2 = 149$ bar. This pO_2 is near the maximum of previously reported growths, which have been carried out over a broad range in pO_2, from 30 bar up to 150 bar (the maximum only being set by the capability of the furnace employed). Crystallinity of the as-grown boule was established via high energy X-ray diffraction. Figure 1 shows the evolution of crystallinity during the crystal growth, the success of seeding, and the overall structural quality of the single crystal boule. The four side panels of Figure 1 b-e shows two dimensional images taken at the marked positions from the seed to the end of crystal

growth on the boule (Figure 1a). The patterns of Bragg spots along the length of the boule are consistent with that of the seed crystal, indicating that seeding occurred during the initial stage of crystal growth and that the crystal continued to grow out axially in registry with the seed. The high energy (short wavelength) of the X-rays allows for penetration throughout the thickness of the crystal boule and sampling of the entire beam footprint at each spot in transmission. Therefore, there is both radial and longitudinal growth coherence.

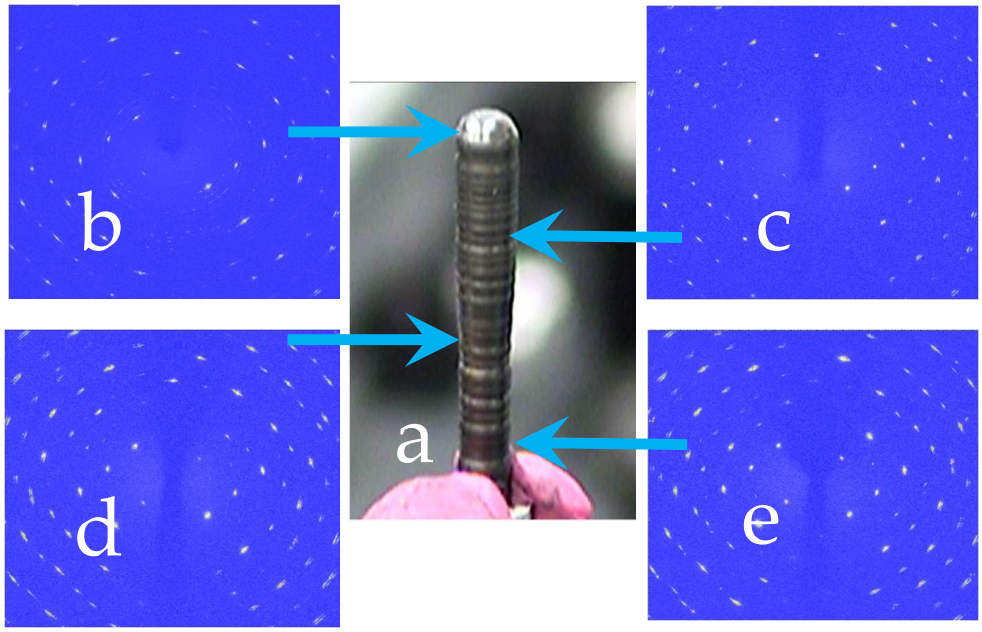

Figure 1. (**a**) $LaNiO_{3-\delta}$ crystal boule grown under pO_2 of 149 bar of oxygen. (**b**–**e**) X-ray single crystal diffraction patterns measured at various locations along the length of the boule at 11-ID-C as indicated by the arrows.

It is well established that oxygen deficiency is common in $RNiO_3$ materials [25,26,28–39], leading to a range of magnetic properties. Most relevant to the present case, both FM and AFM oxygen-deficient phases have been reported in polycrystalline $LaNiO_{3-\delta}$ samples [25,26]. Recently, Wang et al., demonstrated that both AFM ($T_N \approx 150$ K) and FM phases ($T_C \approx 225$ K) could be induced by systematic reduction of the oxygen content in single crystals [24]. To study the impact of such oxygen inhomogeneity in the grown single crystal, we have measured $\chi(T)$ on nine specimens spanning the cross-section of a slice of the boule, as identified in Figure 2a. We found that the $\chi(T)$ behavior of the individual pieces fell into one of two categories, both shown in Figure 2b. The first type of behavior is demonstrated by sample #5. This sample, which was extracted from the axial center of the slice, exhibits a sharp drop in χ below ≈150 K, signaling the entry to an AFM state. We note that this behavior is qualitatively the same as that reported by Guo, et al. [21], who identified the AFM as intrinsic to $LaNiO_3$. The second type of behavior was observed in all other specimens, which were extracted from the periphery of the boule rather than the center. As represented by sample #1, these specimens show a smoothly varying χ and the broad maximum centered near 200 K that has been universally observed in $LaNiO_3$ single crystals grown at all three institutions [20–22]. An abrupt Curie-Weiss tail below 10 K, which is typically observed in $LaNiO_3$, was also observed, which likely arises from a small concentration of spins extrinsic to $LaNiO_3$. Data for all samples can be found in SM Figure S2.

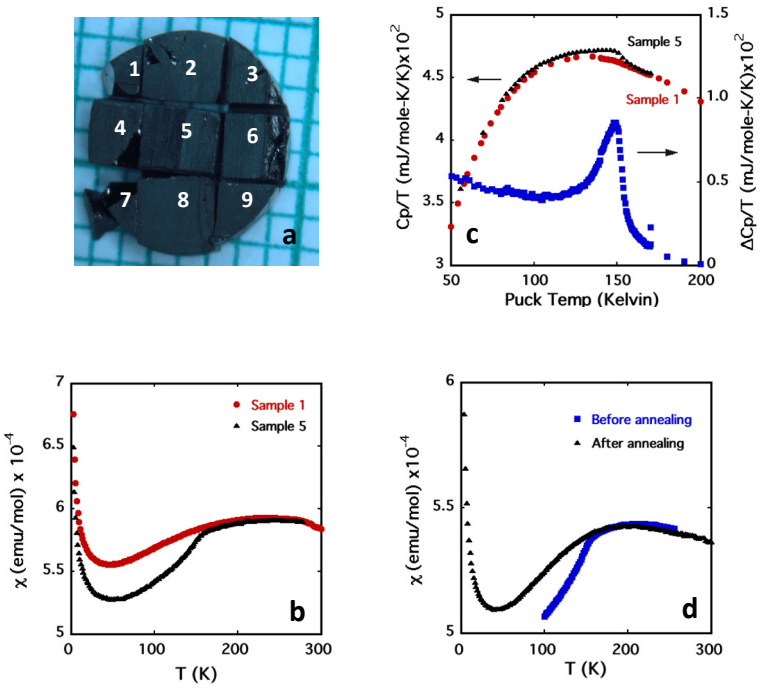

Figure 2. (**a**) Identification of the pieces of $LaNiO_{3-\delta}$ single crystal samples cut from the slice of crystal boule. (**b**) Magnetic susceptibility (χ) vs. temperature (T) for samples #1 and #5. (**c**) Heat capacity (C_p) divided by T for samples #1 and #5. The difference between #5 and #1 is shown in blue squares on the right vertical axis. (**d**) χ vs. T for a piece of sample #5 before and after high pressure oxygen annealing.

Figure 2c shows C_p of samples #1 and #5, plotted as C_p/T vs. T. Consistent with the χ, sample #5 exhibits an anomaly at ≈150 K in C_p/T that is absent in sample #1. The difference between the measurements, also plotted in Figure 2c as $\Delta C_p/T$, clearly shows a broad maximum, the peak center corresponding to T_N. Taken together, these data point to a compositional gradient in the as-grown boule. A similar feature was reported by Guo et al., albeit with a much narrower peak [21]. It is possible that the breadth of our peak can be attributed to a gradient in oxygen content variation along the radius of the boule, arising from the kinetics of oxygen diffusion during the crystal growth. The combined susceptibility and heat capacity data suggest that such kinetics lead to a greater oxygen deficiency in the axial center of the boule compared to the edge, since the AFM transition exhibited by sample #5 is akin to that of the known ordered oxygen vacancy compound $La_2Ni_2O_5$. This naturally leads us to suppose that the samples extracted from outside of the crystal boule behave more closely to the intrinsic behavior of $LaNiO_3$ than those in the center.

While the mechanism described above is a plausible explanation for the inhomogeneous magnetic behavior in the boule, it is also possible that the variation arises not from oxygen inhomogeneity, but rather from cation inhomogeneity distributed radially during growth. To distinguish between these possibilities, we took approximately half of sample #5 (axial center) and performed additional measurements. After re-measuring χ, we annealed it under 150 bar of oxygen at 600 °C for 12 h, followed by slow cooling in the high pO_2 atmosphere at 5 °C/h. At 600 °C, the temperature is high enough to promote oxygen diffusion but too low to engender significant long-range cation diffusion on this timescale. We note that the defect phases of interest ($La_2Ni_2O_5$ and $La_4Ni_4O_{11}$) possess 1:1 La:Ni cation stoichiometry so that probes such as electron dispersive X-ray spectroscopy would not be expected to be an effective means to defect phase inhomogeneity. Figure 2d shows the temperature dependence of χ before (blue squares) and after (black triangles) annealing. Clearly the AFM transition at ≈150 K is suppressed by the high-pressure oxygen annealing, which further supports our assertion that the AFM order is associated with oxygen deficiency.

Given the different magnetic behaviors that we attribute to oxygen vacancies, we used single crystal X-ray diffraction to further investigate the ordering of oxygen vacancies for sample #1 and sample #5. Figure 3a,b shows diffraction data in the pseudocubic $hk0$ and $hk\frac{1}{2}$ planes, respectively, for sample #1. The $hk0$ plane is dominated by Bragg reflections with integer indices; peaks with half or quarter odd integer indices are not apparent. The observed pattern is that expected for a twinned rhombohedral ($R\bar{3}c$) crystal. The $hk\frac{1}{2}$ plane is populated by peaks at R points, where h and k are both half odd integers. Again, this is expected for a rhombohedral crystal. The $R\bar{3}c$ space group expresses a special extinction condition where allowed R points must not possess $|h| = |k| = |l|$. Violations of this condition are apparent in Figure 3b (e.g., at $\frac{1}{2}\frac{1}{2}\frac{1}{2}$). As we have previously pointed out [24], these violations may result from multiple scattering, as is often observed in perovskites [40–43]. In contrast, the diffraction data from sample #5, shown in Figure 3c,d for the $hk0$ plane and $hk\frac{1}{2}$ planes, respectively, differ markedly from that of sample #1. For instance, in the $hk0$ plane, in addition to the integer indexed peaks, there are peaks at half-integer and quarter-integer positions. Similarly, in the $hk\frac{1}{2}$ plane, in addition to the peaks at R points, there are also peaks indexed at X and M points. Additionally, there are peaks indexed with quarter integer indices. These quarter integer peaks indicate an increased unit cell size that arises from oxygen vacancy ordering, and are consistent with the $La_4Ni_4O_{11}$ phase previously observed by electron diffraction [32]. We note that the $La_2Ni_2O_5$ phase, whose presence has been established by the Néel transition observed in χ of sample #5, produces Bragg reflections which are a subset of the $La_4Ni_4O_{11}$ superlattice peaks. Thus, its presence cannot be unambiguously identified in this diffraction measurement [32]. What is clear is that there is a superstructure present in sample #5 that is absent in sample #1.

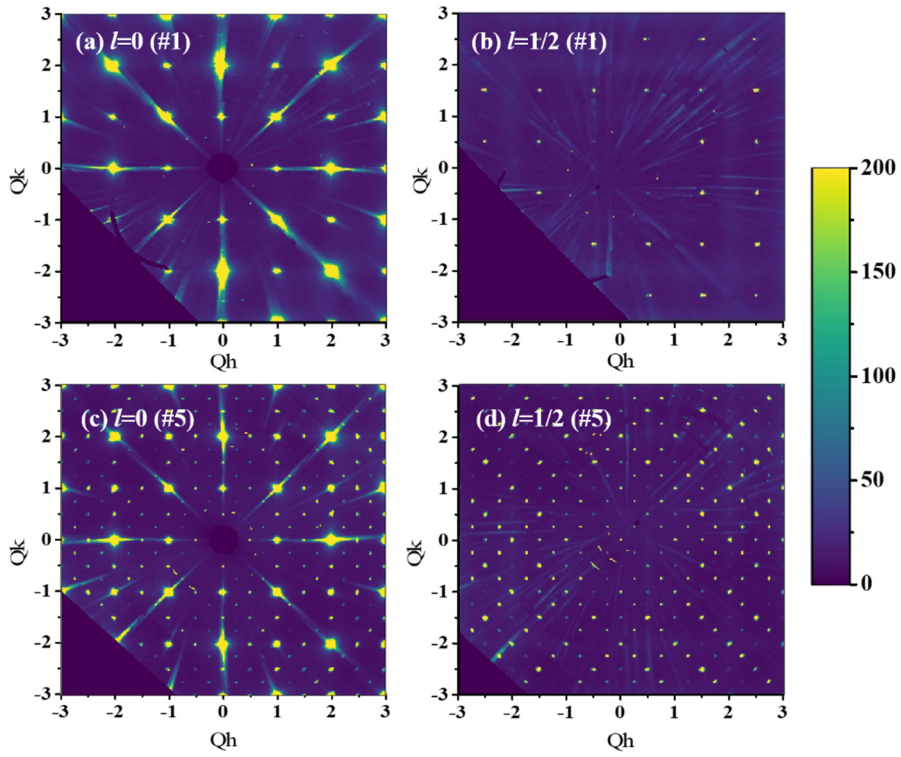

Figure 3. Single crystal X-ray diffraction measured on Sector 6-ID-D in the pseudocubic $hk0$ and $hk\frac{1}{2}$ planes for (**a**,**b**) sample #1 and (**c**,**d**) sample #5. Notice the additional reflections that appear for sample #5 in both planes, indicating that it has an oxygen vacancy ordered superstructure that is not present in sample #1.

To further confirm our findings, we carried out additional annealing experiments. We began with an as-grown specimen (an additional piece not shown in Figure 1), and measured $\chi(T)$. As shown in Figure 4, this piece did not possess an obvious AFM phase transition because no anomaly was observed

at ≈150 K. We then annealed the specimen at 350 °C for 5 days under a reducing atmosphere, a 4% H_2/N_2 mixture. This is the same specimen described in Ref. [24]. We note that, as has been previously mentioned, this type of reduction is expected to yield a non-uniform core-shell like structure with more reduction occurring in the shell [24]. Upon reduction, this piece showed a clear AFM transition (Figure 4). One clearly notable difference between the susceptibility after intentional reduction and the susceptibility of the as-grown piece #5 discussed above is the anomaly at ≈225 K that is only apparent after the intentional reduction. In Ref. [24], we attributed this anomaly to ferromagnetic $La_4Ni_4O_{11}$ ($LaNiO_{2.75}$), which would be consistent with Ref. [37]. However, we clearly see the signature of the $La_4Ni_4O_{11}$ phase via X-ray diffraction in single crystal sample #5, in which no 225 K anomaly was found. These findings in combination would suggest that the ferromagnetism seen in the intentionally reduced specimen may actually arise from a different phase with $0.25 < \delta < 0.5$. This would be consistent with the prior work of Moriga et al. [26,36] who identified the FM phase as $\delta = 0.4$. We are led to speculate that under the closer-to-equilibrium conditions of high temperature, high pO_2 crystal growth, more stable, stoichiometric line phases, etc., $La_2Ni_2O_5$ and $La_4Ni_4O_{11}$ precipitate, while under aggressively non-equilibrium conditions of low temperature H_2-reduction that non-stoichiometric phases, ferromagnetic samples with $\delta \approx 0.4$ can be kinetically trapped within an inhomogeneous core-shell structure. A more developed explanation of this notion is provided in Section III of SM.

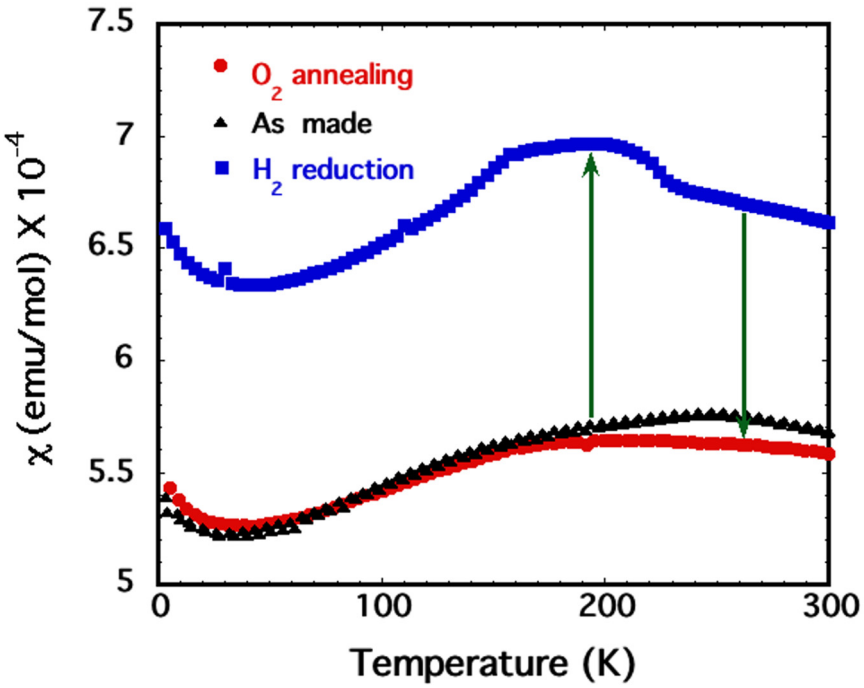

Figure 4. Susceptibility (χ) vs. temperature measurements for an as-grown specimen, after reduction under 4% hydrogen, and then after subsequent high-pressure oxygen annealing.

In a final experiment, the H_2-reduced specimen was annealed under 150 bar of oxygen at 600 °C for 12 h, followed by slow cooling at 5 °C/h. In this specimen, the signature of the phase transition disappeared, and the low temperature χ overlaps closely with that of the original as-grown piece. This annealing sequence establishes the reversibility of the reduction process via high pressure re-oxygenation. We conclude from these experiments that the magnetic anomalies that arise from oxygen-deficient phases can be reversibly converted to nearly stoichiometric $LaNiO_3$.

4. Conclusions

Single crystals of $LaNiO_{3-\delta}$ were grown using a high-pressure floating zone image furnace under 149 bar of pure oxygen. The oxygen inhomogeneity within a cross-sectional slice of the crystal was

characterized by its effects on χ, C_p, and the crystal structure. The results comport with the formation of a radial compositional gradient that results from mass transport kinetics during growth. The area closest to the center of the growth axis possesses regions where oxygen vacancy superstructures exist in the as-grown crystal, whereas the concentrations of these superstructures are greatly diminished towards the periphery to the point where we see no evidence of them. Furthermore, we have shown that the magnetic and thermodynamic properties of single crystal $LaNiO_{3-\delta}$ can be reversibly manipulated via annealing in reducing or oxidizing conditions that modify the nature and concentration of ordered oxygen vacancy phases.

Supplementary Materials: The following are available online at http://www.mdpi.com/2073-4352/10/7/557/s1, Figure S1 Crystal structures of $La_2Ni_2O_5$ and $La_4Ni_4O_{11}$; Figure S2: Magnetic susceptibility (χ) vs Temperature for samples #1 to #9; Figure S3. Proposed phase behavior of the oxygen-deficient perovskite system, $LaNiO_{3-\delta}$. Figure S4. Schematic free energy diagrams for oxygen-deficient phases.

Author Contributions: Conceptualization, J.F.M. and D.P.; methodology, H.Z.; investigation, H.Z., B.-X.W., J.Z., Y.R., M.J.K., S.R., R.O.; writing—H.Z., D.P., J.F.M.; project administration, J.F.M.; funding acquisition, J.F.M. All authors have read and agreed to the published version of the manuscript.

Funding: This work was supported by the US Department of Energy, Office of Science, Basic Energy Sciences, Materials Science and Engineering Division. This research used resources of the Advanced Photon Source, a U.S. Department of Energy (DOE) Office of Science User Facility operated for the DOE Office of Science by Argonne National Laboratory under Contract No. DE-AC02-06CH11357.

Conflicts of Interest: The authors declare no conflict of interest.

References

1. Mazin, I.I.; Khomskii, D.I.; Lengsdorf, R.; Alonso, J.A.; Marshall, W.G.; Ibberson, R.M.; Abd-Elmeguid, M.M. Charge ordering as alternative to Jahn-Teller distortion. *Phys. Rev. Lett.* **2007**, *98*, 176406. [CrossRef]
2. Zhou, J.S.; Marshall, L.G.; Goodenough, J.B. Mass enhancement versus Stoner enhancement in strongly correlated metallic perovskites: $LaNiO_3$ and $LaCuO_3$. *Phys. Rev. B* **2014**, *89*, 245138. [CrossRef]
3. Disa, A.S.; Walker, F.J.; Ismail-Beigi, S.; Ahn, C.H. Research Update: Orbital polarization in $LaNiO_3$-based heterostructures. *APL Mater.* **2015**, *3*, 062303. [CrossRef]
4. Medarde, M.; Fernández-Díaz, M.T.; Lacorre, P. Long-range charge order in the low-temperature insulating phase of $PrNiO_3$. *Phys. Rev. B* **2008**, *78*, 212101. [CrossRef]
5. Allen, S.J.; Hauser, A.J.; Mikheev, E.; Zhang, J.Y.; Moreno, N.E.; Son, J.; Stemmer, S. Gaps and pseudogaps in perovskite rare earth nickelates. *APL Mater.* **2015**, *3*, 062503. [CrossRef]
6. Lee, S.; Chen, R.; Balents, L. Metal-insulator transition in a two-band model for the perovskite nickelates. *Phys. Rev. B* **2011**, *84*, 165119. [CrossRef]
7. Green, R.J.; Haverkort, M.W.; Sawatzky, G.A. Bond disproportionation and dynamical charge fluctuations in the perovskite rare-earth nickelates. *Phys. Rev. B* **2016**, *94*, 195127. [CrossRef]
8. Park, H.; Millis, A.J.; Marianetti, C.A. Site-selective Mott transition in rare-earth-element nickelates. *Phys. Rev. Lett.* **2012**, *109*, 156402. [CrossRef]
9. Johnston, S.; Mukherjee, A.; Elfimov, I.; Berciu, M.; Sawatzky, G.A. Charge disproportionation without charge transfer in the rare-earth-element nickelates as a possible mechanism for the metal-insulator transition. *Phys. Rev. Lett.* **2014**, *112*, 106404. [CrossRef]
10. Bisogni, V.; Catalano, S.; Green, R.J.; Gibert, M.; Scherwitzl, R.; Huang, Y.; Sawatzky, G. Ground-state oxygen holes and the metal–insulator transition in the negative charge-transfer rare-earth nickelates. *Nat. Commun.* **2016**, *7*, 1–8. [CrossRef]
11. Mizokawa, T.; Khomskii, D.; Sawatzky, G. Spin and charge ordering in self-doped Mott insulators. *Phys. Rev. B* **2000**, *61*, 11263. [CrossRef]
12. Varignon, J.; Grisolia, M.N.; Iniguez, J.; Barthélémy, A.; Bibes, M. Complete phase diagram of rare-earth nickelates from first-principles. *NPJ Quantum Mater.* **2017**, *2*, 1–9. [CrossRef]
13. Shamblin, J.; Heres, M.; Zhou, H.; Sangoro, J.; Lang, M.; Neuefeind, J.; Johnston, S. Experimental evidence for bipolaron condensation as a mechanism for the metal-insulator transition in rare-earth nickelates. *Nat. Commun.* **2018**, *9*, 1–7. [CrossRef] [PubMed]

14. Li, B.; Louca, D.; Yano, S.; Marshall, L.G.; Zhou, J.; Goodenough, J.B. Insulating pockets in metallic $LaNiO_3$. *Adv. Electron. Mater.* **2016**, *2*, 1500261. [CrossRef]
15. Torrance, J.B.; Lacorre, P.; Nazzal, A.I.; Ansaldo, E.J.; Niedermayer, C. Systematic study of insulator-metal transitions in perovskites $RNiO_3$ (R = Pr, Nd, Sm, Eu) due to closing of charge-transfer gap. *Phy. Rev. B* **1992**, *45*, 8209. [CrossRef]
16. Shannon, R.D. Revised effective ionic radii and systematic studies of interatomic distances in halides and chalcogenides. *Acta Crystallogr. Sect. A* **1976**, *32*, 751–767. [CrossRef]
17. Goodenough, J.B.; Raccah, P.M. Complex vs band formation in perovskite oxides. *J. Appl. Phys.* **1965**, *36*, 1031–1032. [CrossRef]
18. Sreedhar, K.; Honig, J.M.; Darwin, M.; McElfresh, M.; Shand, P.M.; Xu, J.; Spalek, J. Electronic properties of the metallic perovskite $LaNiO_3$: Correlated behavior of 3d electrons. *Phys. Rev. B* **1992**, *46*, 6382. [CrossRef]
19. Vasanthacharya, N.Y.; Ganguly, P.; Goodenough, J.B.; Rao, C.N.R. Valence states and magnetic properties of $LaNi_{1-x}Mn_xO_3$ (for $0 \leqslant x \leqslant 0.2$ and $x = 0.5$). *J. Phy. C Solid State Phys.* **1984**, *17*, 2745. [CrossRef]
20. Zhang, J.; Zheng, H.; Ren, Y.; Mitchell, J.F. High-pressure floating-zone growth of perovskite nickelate $LaNiO_3$ single crystals. *Cryst. Growth Des.* **2017**, *17*, 2730–2735. [CrossRef]
21. Meng, N.; Ren, X.; Santagiuliana, G.; Ventura, L.; Zhang, H.; Wu, J.; Bilotti, E. Ultrahigh β-phase content poly (vinylidene fluoride) with relaxor-like ferroelectricity for high energy density capacitors. *Nat. Commun.* **2019**, *10*, 1–9. [CrossRef] [PubMed]
22. Dey, K.; Hergett, W.; Telang, P.; Abdel-Hafiez, M.M.; Klingeler, R. Magnetic properties of high-pressure optical floating-zone grown $LaNiO_3$ single crystals. *J. Cryst. Growth* **2019**, *524*, 125157. [CrossRef]
23. Zheng, H.; Zhang, J.; Wang, B.; Phelan, D.; Krogstad, M.J.; Ren, Y.; Mitchell, J.F. High pO_2 Floating Zone Crystal Growth of the Perovskite Nickelate $PrNiO_3$. *Crystals* **2019**, *9*, 324. [CrossRef]
24. Wang, B.X.; Rosenkranz, S.; Rui, X.; Zhang, J.; Ye, F.; Zheng, H.; Phelan, D. Antiferromagnetic defect structure in $LaNiO_{3-\delta}$ single crystals. *Phys. Rev. Mater.* **2018**, *2*, 064404. [CrossRef]
25. Moriga, T.; Usaka, O.; Nakabayashi, I.; Hirashima, Y.; Kohno, T.; Kikkawa, S.; Kanamaru, F. Reduction of the perovskite-type $LnNiO_3$ (*Ln* = Pr, Nd) to $Ln_3Ni_3O_7$ with monovalent nickel ions. *Solid State Ionics* **1994**, *74*, 211. [CrossRef]
26. Moriga, T.; Usaka, O.; Imamura, T.; Nakabayashi, I.; Matsubara, I.; Kinouchi, T.; Kanamaru, F. Synthesis, Crystal Structure, and Properties of Oxygen-Deficient Lanthanum Nickelate $LaNiO_{3-x}$ ($0 \leq x \leq 0.5$). *Bull. Chem. Soc. Jpn.* **1994**, *67*, 687–693. [CrossRef]
27. Zhang, J.; Phelan, D.; Botana, A.S.; Chen, Y.S.; Zheng, H.; Krogstad, M.; Rosenkranz, S. Intertwined density waves in a metallic nickelate. *arXiv* **2020**, arXiv:2004.07897.
28. Abbate, M.; Zampieri, G.; Prado, F.; Caneiro, A.; Gonzalez-Calbet, J.M.; Vallet-Regi, M. Electronic structure and metal-insulator transition in $LaNiO_{3-\delta}$. *Phys. Rev. B* **2002**, *65*, 155101. [CrossRef]
29. Alonso, J.A.; Martínez-Lope, M.J. Preparation and crystal structure of the deficient perovskite $LaNiO_{2.5}$, solved from neutron powder diffraction data. *J. Chem. Soc. Dalton Trans.* **1995**, *17*, 2819–2824. [CrossRef]
30. Alonso, J.A.; Martínez-Lope, M.J.; García-Muñoz, J.L.; Fernández-Díaz, M.T. A structural and magnetic study of the defect perovskite from high-resolution neutron diffraction data. *J. Phys. Condens. Matter.* **1997**, *9*, 6417. [CrossRef]
31. Crespin, M.; Levitz, P.; Gatineau, L. Reduced Forms of $LaNi0_3$ Perovskite Part 1.-Evidence for New Phases: $La_2Ni_2O_5$ and $LaNiO_2$. *J. Chem. Soc. Faraday Trans. 2* **1983**, *79*, 1181–1194. [CrossRef]
32. Gonzalez-Calbet, J.M.; Sayagues, M.J.; Vallet-Regi, M. An electron diffraction study of new phases in the $LaNiO_{3-x}$ system. *Solid State Ionics.* **1989**, *32*, 721726. [CrossRef]
33. Levitz, P.; Crespin, M.; Gatineau, L. Reduced forms of $LaNiO_3$ perovskite. Part 2.—X-ray structure of $LaNiO_2$ and extended X-ray absorption fine structure study: Local environment of monovalent nickel. *J. Chem. Soc. Faraday Trans.* **1983**, *79*, 1195. [CrossRef]
34. Middey, S.; Rivero, P.; Meyers, D.; Kareev, M.; Liu, X.; Cao, Y.; Chakhalian, J. Polarity compensation in ultra-thin films of complex oxides: The case of a perovskite nickelate. *Sci. Rep.* **2014**, *4*, 1–7. [CrossRef]
35. Moriga, T.; Kikkawa, S.; Takahashi, M.; Kanamaru, F.; Nakabayashi, I. XAFS study on reduction process of Pauli-paramagnetic $LaNiO_3$ to antiferromagnetic $La_2Ni_2O_5$. *Jpn. J. Appl. Phys.* **1993**, *32*, 764. [CrossRef]
36. Moriga, T.; Usaka, O.; Nakabayashi, I.; Kinouchi, T.; Kikkawa, S.; Kanamaru, F. Characterization of oxygen-deficient phases appearing in reduction of the perovskite-type $LaNiO_3$ to $La_2Ni_2O_5$. *Solid State Ionics.* **1995**, *79*, 252. [CrossRef]

37. Sanchez, R.D.; Causa, M.T.; Caneiro, A.; Butera, A.; Vallet-Regi, M.; Sayagues, M.J.; Rivas, J. Metal-insulator transition in oxygen-deficient $LaNiO_{3-x}$ perovskites. *Phys. Rev. B* **1996**, *54*, 16574. [CrossRef]
38. Rao, C.N.R.; Gopalakrishnan, J.; Vidyasagar, K.; Ganguli, A.K.; Ramanan, A.; Ganapathi, L. Novel metal oxides prepared by ingenious synthetic routes. *J. Mater. Res.* **1986**, *1*, 280. [CrossRef]
39. Vidyasagar, K.; Reller, A.; Gopalakrishnan, J.; Rao, C.N.R. Oxygen Vacancy Ordering in Superlattices of the Two Novel Oxides, $La_2Ni_2O_5$ and $La_2Co_2O_5$, prepared by Low Temperature Reduction of the Parent Perovskites. *J. Chem. Soc. Chem. Commun.* **1985**, *1*, 7–8. [CrossRef]
40. Phelan, D.; Long, X.; Xie, Y.; Ye, Z.G.; Glazer, A.M.; Yokota, H.; Gehring, P.M. Single crystal study of competing rhombohedral and monoclinic order in lead zirconate titanate. *Phys. Rev. Lett.* **2010**, *105*, 207601. [CrossRef]
41. Phelan, D. Constraints on the possible long-range orbital ordering in $LaCoO_3$. *J. Magn. Magn. Mater.* **2014**, *350*, 183. [CrossRef]
42. Shirane, G.; Shapiro, S.M.; Tranquada, J.M. *Neutron Scattering with a Triple-Axis Spectrometer: Basic Techniques*; Cambridge University Press: Cambridge, UK, 2002.
43. Ge, W.; Devreugd, C.P.; Phelan, D.; Zhang, Q.; Ahart, M.; Li, J.; Gehring, P.M. Lead-free and lead-based ABO3 perovskite relaxors with mixed-valence A-site and B-site disorder: Comparative neutron scattering structural study of $(Na_{1/2}Bi_{1/2})$ TiO_3 and $Pb(Mg_{1/3}Nb_{2/3})O_3$. *Phys. Rev. B* **2013**, *88*, 174115. [CrossRef]